Cytosolic inositol 1,4,5-trisphosphate dynamics during intracellular calcium oscillations in living cells

Toru Matsu-ura,[1] Takayuki Michikawa,[1,2,3] Takafumi Inoue,[2,3] Atsushi Miyawaki,[4] Manabu Yoshida,[3,5] and Katsuhiko Mikoshiba[1,2,3]

[1]Laboratory for Developmental Neurobiology, Brain Science Institute, RIKEN, Saitama 351-0198, Japan
[2]Division of Molecular Neurobiology, Department of Basic Medical Sciences, Institute of Medical Science, University of Tokyo, Tokyo 108-8639, Japan
[3]Calcium Oscillation Project, International Cooperative Research Project—Solution Oriented Research for Science and Technology, Japan Science and Technology Agency, Saitama 332-0012, Japan
[4]Laboratory for Cell Function and Dynamics, Advanced Technology Development Center, Brain Science Institute, RIKEN, Saitama 351-0198, Japan
[5]Misaki Marine Biological Station, Graduate School of Science, University of Tokyo, Kanagawa, 238-0225, Japan

We developed genetically encoded fluorescent inositol 1,4,5-trisphosphate (IP_3) sensors that do not severely interfere with intracellular Ca^{2+} dynamics and used them to monitor the spatiotemporal dynamics of both cytosolic IP_3 and Ca^{2+} in single HeLa cells after stimulation of exogenously expressed metabotropic glutamate receptor 5a or endogenous histamine receptors. IP_3 started to increase at a relatively constant rate before the pacemaker Ca^{2+} rise, and the subsequent abrupt Ca^{2+} rise was not accompanied by any acceleration in the rate of increase in IP_3. Cytosolic [IP_3] did not return to its basal level during the intervals between Ca^{2+} spikes, and IP_3 gradually accumulated in the cytosol with a little or no fluctuations during cytosolic Ca^{2+} oscillations. These results indicate that the Ca^{2+}-induced regenerative IP_3 production is not a driving force of the upstroke of Ca^{2+} spikes and that the apparent IP_3 sensitivity for Ca^{2+} spike generation progressively decreases during Ca^{2+} oscillations.

Introduction

An increase in cytosolic [Ca^{2+}] ([Ca^{2+}]$_c$) is a ubiquitous intracellular signal that controls various cellular processes, including fertilization, proliferation, development, learning and memory, contraction, and secretion (Berridge et al., 2000). [Ca^{2+}]$_c$ rises evoked by extracellular stimuli are often observed in the form of pulsatile Ca^{2+} spikes that result from the transient opening of Ca^{2+} channels located either in the plasma membrane or on the cytosolic Ca^{2+} stores (Berridge and Dupont, 1994). The spatial counterpart of Ca^{2+} spikes are Ca^{2+} waves, which are produced when an initial localized [Ca^{2+}]$_c$ elevation leads to the propagation of the rise in [Ca^{2+}]$_c$ throughout the cytoplasm (Lechleiter et al., 1991; Thomas et al., 1991). The frequency of the occurrence of Ca^{2+} spikes is correlated with the stimulus intensity (Woods et al., 1986; Berridge, 1988; Jacob et al., 1988; Prentki et al., 1988), and the time course of an individual Ca^{2+} spike depends on the type of receptor stimulated but not on the stimulus intensity (Cobbold et al., 1991; Thomas et al., 1991), indicating that the information of both the stimulus species and its intensity is encoded within the temporal pattern of cytosolic Ca^{2+}.

Stimulus-induced cytosolic Ca^{2+} spikes usually form as a result of an initial slow pacemaker rise in [Ca^{2+}]$_c$ followed by a rapid rise in [Ca^{2+}]$_c$ (Jacob et al., 1988; Thomas et al., 1991; Bootman and Berridge, 1996). The rate of the rapid [Ca^{2+}]$_c$ rise remains relatively constant regardless of the stimulus intensity (Cobbold et al., 1991; Thomas et al., 1991), suggesting that a regenerative process is involved in the generation of the abrupt upstroke (Thomas et al., 1991). Such regenerative processes require a positive-feedback element (Meyer and Stryer, 1991), and some molecules that are critical to the regenerative process have been proposed. PLC catalyzes the formation of inositol 1,4,5-trisphosphate (IP_3) and diacylglycerol from phosphatidylinositol 4,5-bisphosphate and has been hypothesized to act as a positive-feedback element (Meyer and Stryer, 1988; Harootunian et al., 1991) because its activity is stimulated by cytosolic Ca^{2+}

Correspondence to Takayuki Michikawa: takamich@ims.u-tokyo.ac.jp; or Katsuhiko Mikoshiba: mikosiba@ims.u-tokyo.ac.jp

Abbreviations used in this paper: [Ca^{2+}]$_c$, cytosolic Ca^{2+} concentration; C-PHD, cyan fluorescent protein–fused PHD; ECFP, enhanced cyan fluorescent protein; IP_3, inositol 1,4,5-trisphosphate; [IP_3]$_c$, cytosolic IP_3 concentration; IP_3R, IP_3 receptor; IRIS, IP_3R-based IP_3 sensor; mGluR, metabotropic glutamate receptor; PHD, pleckstrin homology domain; V-PHD, Venus-fused PHD.

The online version of this article contains supplemental material.

The Journal of Cell Biology, Vol. 173, No. 5, June 5, 2006 755–765
http://www.jcb.org/cgi/doi/10.1083/jcb.200512141

(Rebecchi and Pentyala, 2000). According to their hypothesis, the positive-feedback regulation of PLC by cytosolic Ca^{2+} allows generation of IP_3 spikes that result in Ca^{2+} spikes through activation of the IP_3 receptor (IP_3R)/IP_3-gated Ca^{2+} release channel (Meyer and Stryer, 1988). Another hypothesis is that the positive-feedback regulation is attributable to the intrinsic property of the IP_3R. The biphasic dependency of channel activity on Ca^{2+} (Iino, 1990) may create the rapid upstroke of Ca^{2+} spikes even at constant levels of IP_3 (Wakui et al., 1989; Osipchuk et al., 1990; Wakui et al., 1990; Dupont et al., 1991; De Young and Keizer, 1992; Hajnoczky and Thomas, 1997). These mechanisms for the generation of Ca^{2+} spikes, however, are not necessarily exclusive, and combined models are also plausible.

Observation of cytosolic IP_3 dynamics during Ca^{2+} spikes should help us better understand the mechanism responsible for the Ca^{2+} spike generation (Meyer and Stryer, 1991). The GFP-tagged pleckstrin homology domain (PHD) of PLC-δ1, which interacts with phosphatidylinositol 4,5-bisphosphate and/or IP_3, has been used to monitor IP_3 production and its oscillatory translocation from plasma membrane to the cytosol synchronously with Ca^{2+} oscillation was observed in MDCK cells (Hirose et al., 1999), suggesting that each Ca^{2+} spike accompanies IP_3 production. However, there is no simple correlation between its translocation from the plasma membrane to the cytosol and actual cytosolic [IP_3] ([IP_3]$_c$ van der Wal et al., 2001; Xu et al., 2003; Irvine, 2004). Fluorescent IP_3 sensors based on the IP_3 binding domain of IP_3R have recently been developed (Tanimura et al., 2004; Sato et al., 2005; Remus et al., 2006), but no one has ever used them to investigate the mechanism underlying the Ca^{2+} spike generation in living cells.

In the present study, we developed low IP_3 binding affinity, high signal-to-noise ratio cytosolic IP_3 sensors based on the IP_3 binding domain of mouse type 1 IP_3R (IP_3R1) and used them to analyze the mechanism responsible for the generation of Ca^{2+} oscillations. Simultaneous imaging of [Ca^{2+}]$_c$ and [IP_3]$_c$ in living cells exposed to extracellular stimuli provided us with a novel insight into the mechanism of generation of intracellular Ca^{2+} spikes.

Results

Development of cytosolic IP_3 sensors based on the IP_3 binding domain of IP_3R1

To develop cytosolic IP_3 sensors, we constructed tandem fusion proteins of a variant of yellow fluorescent protein, Venus (Nagai et al., 2002); an IP_3 binding domain of IP_3R1 (Miyawaki et al., 1991; Yoshikawa et al., 1996; Bosanac et al., 2002); and an enhanced cyan fluorescent protein (ECFP; Fig. 1 A). We used

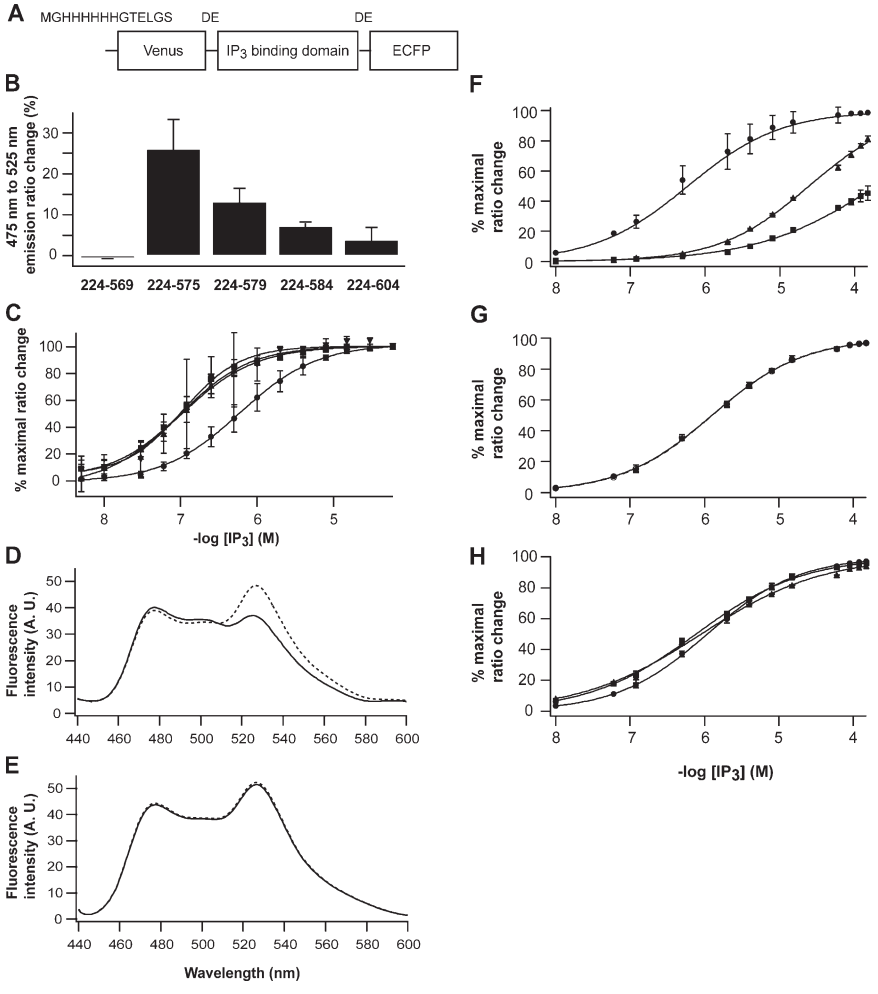

Figure 1. **IP_3 sensor proteins based on the IP_3 binding domain of mouse IP_3R1.** (A) A basic design for IP_3 sensors. (B) ECFP/Venus emission ratio changes of IP_3 sensors in COS7 lysates after the addition of 60 μM of IP_3. (C) Apparent IP_3 affinity of IP_3 sensors composed with amino acid residues 224–575 (circle), 224–579 (triangle), 224–584 (square), and 224–604 (inverse triangle) in COS7 lysates. Data were obtained from three independent measurements. Emission spectra of purified IRIS-1 (D) and IRIS-1–Dmut (E) excited at 420 nm with 0 μM (broken line) and 100 μM (solid line) of IP_3. Measurements were performed at 20°C in buffer A (10 mM Hepes, pH 7.2, 100 mM NaCl, 1 mM 2-mercaptoethanol, and 0.5% NP-40) containing 1 mM EDTA. (F) Specificity of IRIS-1 against IP_3 (circle) and its natural metabolites, 1,3,4,5 IP_4 (triangle) and 1,4 IP_2 (square). Measurements were performed at 20°C in buffer A containing 1 mM EDTA. (G) Ca^{2+} sensitivity of IRIS-1. Emission of IRIS-1 was measured in buffer A containing 1 mM HEDTA (circle) or 1 μM free Ca^{2+} (square). The free Ca^{2+} concentration was adjusted as described elsewhere (Michikawa et al., 1999). (H) pH sensitivity of IRIS-1. Three buffers with different pH (circle, pH 7.0; square, pH 7.4; triangle, pH 7.8) were prepared based on buffer A containing 1 mM EDTA. Error bars correspond to the SD (n = 3).

amino acid residues 224–569, 224–575, 224–579, 224–584, and 224–604 of mouse IP_3R1 as an IP_3 binding motif and found that all fusion proteins except the protein composed of residues 224–569 showed IP_3-dependent decrease of fluorescence resonance energy transfer (FRET) between Venus and ECFP (Fig. 1 B). The largest FRET change was obtained in the fusion protein composed of residues 224–575 of mouse IP_3R1, and the 475-nm (ECFP) to 525-nm (Venus) emission ratio of the fusion protein increased by 25.1 ± 8.0% ($n = 3$) after the addition of 60 μM IP_3 into cell lysates. We designated this fusion protein as IP_3R-based IP_3 sensor 1 (IRIS-1). The emission ratio of IRIS-1 changed depending on the concentration of IP_3 applied, but its apparent IP_3 sensitivity (K_d = 549 ± 62 nM; $n = 3$) was significantly lower than those of fusion proteins composed of residues 224–604 (K_d = 107 ± 41 nM; $n = 3$), 224–584 (K_d = 105 ± 0 nM; $n = 3$), and 224–579 (K_d = 95 ± 38 nM; $n = 3$; Fig. 1 C).

We further characterized IRIS-1 in vitro. The protein was expressed in Sf9 cells and was purified as described in Materials and methods. Fig. 1 D shows emission spectrum of IRIS-1 when excited at 420 nm. Addition of 100 μM IP_3 slightly increased the 475-nm (ECFP) emission and decreased the 525-nm (Venus) emission of IRIS-1. We also constructed IRIS-1–Dmut, in which two critical amino acid residues (Thr267 and Lys508) for IP_3 binding have been replaced from IRIS-1, and found that the emission spectrum of IRIS-1–Dmut was unaltered by the addition of 100 μM IP_3 (Fig. 1 E), indicating that FRET between the flanking fluorescent proteins decreased in response to IP_3 binding to the IP_3 binding domain of IRIS-1. The emission change of purified IRIS-1 exhibits an IP_3 sensitivity (K_d = 437 ± 30 nM; $n = 6$) that is slightly higher than that measured in COS7 cell lysates (Fig. 1 F). IRIS-1 can discriminate IP_3 from its natural metabolites, inositol 1,3,4,5-tetrakisphosphate (IP_4) and inositol 1,4-bisphosphate (IP_2), with >50 and >400 times the sensitivity, respectively (Fig. 1 F). The IP_3 sensitivity of IRIS-1 was not influenced by the addition of 1 μM Ca^{2+} (Fig. 1 G). IRIS-1 did not reveal severe pH sensitivity, at least in the range examined (Fig. 1 H).

IRIS-1 was uniformly distributed within the cytosol of intact HeLa cells (Fig. 2 A), and ~80% of IRIS-1 was released from the cells after 5 min of treatment with 0.1% saponin (Fig. 2, A and B). ECFP-tagged IP_3R1, which is an ER resident protein, was hardly released from the cells with the same treatment (Fig. 2, A and B). These results indicate that IRIS-1 is mainly localized in the cytosol of HeLa cells. To monitor cytosolic IP_3 and Ca^{2+} dynamics simultaneously, Indo-1 was loaded into IRIS-1–expressing HeLa cells. Fig. 2 D shows FRET changes of IRIS-1 accompanied by Ca^{2+} transients (Fig. 2 C) elicited by sequential stimulations with 1, 5, and 10 μM of histamine. We did not detect FRET changes in IRIS-1–Dmut–expressing cells even when Ca^{2+} transients were observed (Fig. 2, E and F), and the expression level of IRIS-1–Dmut was indistinguishable from that of IRIS-1 (Fig. 2 G). FRET changes of IRIS-1 were completely blocked by the addition of 10 μM of PLC inhibitor U73122 but not by its inactive analogue U73343 in (Fig. S1, A and B, available at http://www.jcb.org/cgi/content/full/jcb.200512141/DC1). These results indicate that IRIS-1 can monitor $[IP_3]_c$ changes in living cells.

IP_3 dynamics during Ca^{2+} oscillations in HeLa cells

To monitor cytoplasmic IP_3 dynamics during Ca^{2+} oscillations, we introduced both IRIS-1 and metabotropic glutamate receptor 5a (mGluR5a) cDNAs into HeLa cells. The frequency of Ca^{2+} oscillations mediated by mGluR5a is known to depend on the extent of mGluR5a expression (Nash et al., 2002), and the Ca^{2+} oscillation frequency varied from 19 to 72 mHz (45.6 ± 16.0 mHz; $n = 25$) in the cells transfected with mGluR5a cDNA

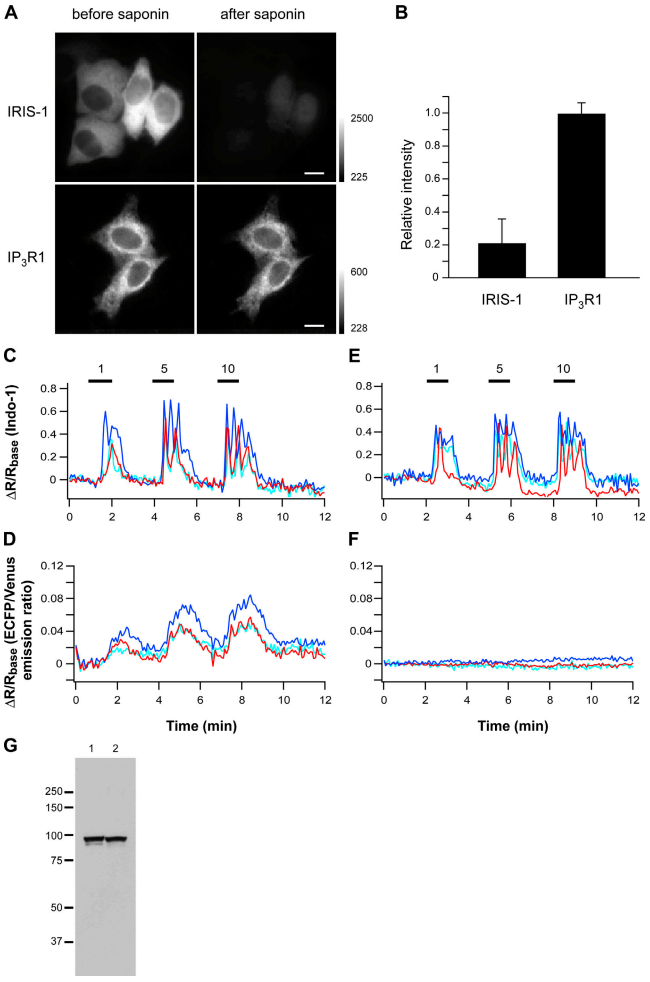

Figure 2. **Characterization of IRIS-1 expressed in HeLa cells.** (A) Intracellular localization of IRIS-1 and ECFP-tagged mouse IP_3R1 shown by the ECFP fluorescence excited at 425–445 nm. Cells were treated with a solution containing 0.1% saponin, 80 mM Pipes, pH 7.2, 1 mM $MgCl_2$, 1 mM EGTA, and 4% polyethylen glycol for 5 min at room temperature and were washed with balanced salt solution for 10 min. Bars, 10 μm. (B) Relative fluorescence intensity of IRIS-1 ($n = 20$) and ECFP-tagged IP_3R1 ($n = 6$) after the saponin treatment. Error bars indicate SD. (C–F) Time courses of emission changes of Indo-1 (C) and IRIS-1 (D) in a single HeLa cell sequentially stimulated with 1, 5, and 10 μM of histamine (horizontal bars). The same experiments were performed in IRIS-1–Dmut–expressing HeLa cells (E and F). Three different color plots represent data from three cells in the same viewing field (C–F). ECFP/Venus emission ratio (IRISs and C/V-PHD) and 420–440/460–510-nm emission ratio (Indo-1) were defined as R, and ΔR was defined as $R - R_{base}$, where R_{base} is the basal level of R, in this and the following figures. (G) Expression levels of IRIS-1 (lane 1) and IRIS-1–Dmut (lane 2) in HeLa cells assessed by Western blot analysis using an anti-GFP antibody. Similar results were observed in three independent experiments. Molecular mass markers are shown on the left ($\times 10^{-3}$).

alone (no IP_3 sensor proteins). IP_3 sensors that can bind IP_3 may perturb IP_3 dynamics in living cells to some extent with their potential to function as an IP_3 buffer. IRIS-1–expressing cells, however, exhibited a Ca^{2+} oscillation frequency (36.9 ± 7.4 mHz; $n = 23$; Fig. 3, A and B) that was not significantly different from the frequency observed in the IRIS-1–Dmut–expressing cells (32.5 ± 11.2 mHz; $n = 17$; Fig. 3, A and B; $P > 0.05$, *t* test). The decay times of each Ca^{2+} spike were also indistinguishable between IRIS-1–expressing cells and IRIS-1–Dmut–expressing cells stimulated with 100 μM glutamate (unpublished data). These results indicate that the expression of IRIS-1 did not have a marked influence on Ca^{2+} dynamics evoked by mGluR5a stimulation. We noticed that the expression of ECFP-fused PHD (C-PHD) and Venus-fused PHD (V-PHD) significantly reduced the Ca^{2+} oscillation frequency (21.5 ± 10.3 mHz; $n = 38$; Fig. 3, A and B) in comparison with the cells expressing mGluR5a alone ($P < 0.05$, *t* test) or mGluR5a plus IRIS-1–Dmut ($P < 0.05$, *t* test), but the expression level of mGluR5a was not reduced in C/V-PHD–expressing cells (Fig. 3 C), indicating that the exogenous expression of PHD perturbs the intracellular Ca^{2+} dynamics evoked by mGluR5a stimulation.

Fig. 4 A shows the IP_3 dynamics monitored by IRIS-1 during Ca^{2+} oscillations in mGluR5a-expressing HeLa cells stimulated with 100 μM of glutamate. Cytosolic IP_3 rapidly increased after the addition of glutamate and was progressively accumulated during Ca^{2+} oscillations evoked by the continuous presence of the stimulus. $[IP_3]_c$ did not return to its basal level within the interspike interval of the Ca^{2+} oscillations in 28 out of 29 cells that exhibited Ca^{2+} oscillation frequencies between 14 and 45 mHz. After the removal of glutamate from the extracellular solution, the $[IP_3]_c$ slowly returned to its basal level, with time constants of 46.8 ± 14.4 s ($n = 31$). The characteristic temporal pattern of the IRIS-1 signals was significantly different from that of the C/V-PHD signals that showed oscillatory changes synchronous to the Ca^{2+} oscillation (Fig. 4 A), as previously reported in MDCK cells (Hirose et al., 1999) and in mGluR5a-expressing CHO cells (Nash et al., 2002). The accumulation of cytosolic IP_3 was also observed in HeLa cells stimulated with 3 μM of histamine (Fig. 4 B), indicating that the IP_3 dynamics that were observed are not specific to mGluR5a-expressing cells. IRIS-1 signals in the cells stimulated with histamine did not show significant fluctuations even when Ca^{2+} oscillations occurred (Fig. 4 B), indicating that the small fluctuations of $[IP_3]_c$ observed in the cells stimulated with 100 μM glutamate (Fig. 4 A) are not required for the generation of Ca^{2+} spikes in HeLa cells. We could not detect any significant PHD signal changes in HeLa cells stimulated with 3 μM of histamine because of the low signal-to-noise ratio of the C/V-PHD signals (unpublished data).

We analyzed the mean IRIS-1 signal at the time of the onset of each Ca^{2+} spike in mGluR5a-expressing HeLa cells stimulated with 100 μM of glutamate and in HeLa cells stimulated with 3 μM of histamine. Fig. 4 C shows that $[IP_3]_c$ at the time of Ca^{2+} spike generation continuously changes during the period of Ca^{2+} oscillations in both cells, indicating that a constant threshold of IP_3 is not involved in the generation of repetitive Ca^{2+} spikes.

We did not detect IP_3 spikes, i.e., rapid upstrokes of $[IP_3]_c$ with a constant amplitude followed by a gradual decrease of $[IP_3]_c$ to its basal level, even when Ca^{2+} spikes were triggered by glutamate (Fig. 4 A) or histamine application (Fig. 4 B). However, if the IP_3 sensor was saturated with IP_3 in the cells and/or the FRET change of IRIS-1 upon IP_3 binding was too slow to detect $[IP_3]_c$ changes, we would have missed the IP_3 spikes, so we conducted the following experiments to investigate these possibilities. IRIS-1–expressing HeLa cells were permeabilized with 60 μM β-escin for 3 min and then exposed to solutions containing various concentrations of IP_3. IRIS-1 exhibited a maximal response of 28.0% after addition of an

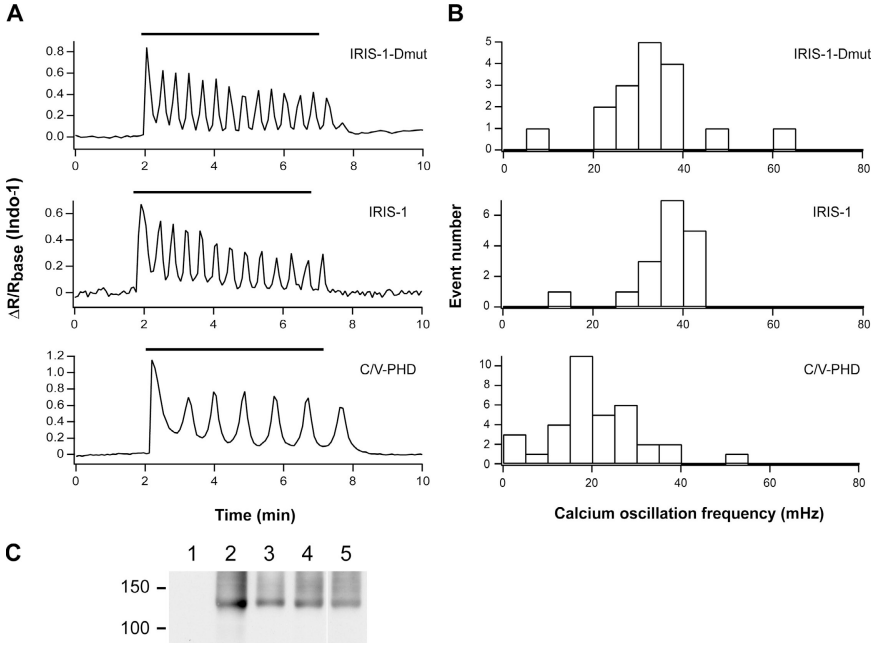

Figure 3. **Effects of exogenously expressed proteins on Ca^{2+} oscillation frequency in mGluR5a-expressing HeLa cells.** (A) Emission ratio change of Indo-1 signals in cells stimulated with 100 μM of glutamate (horizontal bars). (B) Histograms of Ca^{2+} oscillation frequency in mGluR5a-expressing cells stimulated with 100 μM of glutamate. (C) Western blot analysis of cell lysates prepared from HeLa cells transfected with mGluR5a alone (lane 2), mGluR5a plus C/V-PHD (lane 3), mGluR5a plus IRIS-1 (lane 4), or mGluR5a plus IRIS-1–Dmut (lane 5). Nontransfected cells were used as a control (lane 1). An anti-mGluR5 antibody was used. Molecular mass markers are shown on the left ($\times 10^{-3}$).

excess amount of IP_3 under the conditions used (Fig. S1 C). The maximal response observed was greater than that observed in intact cells stimulated with 100 μM glutamate (~20%; Fig. 4 A) and 3 μM histamine (~7%; Fig. 4 B), indicating that the dynamic range of changes in the IRIS-1 signals is greater than the changes in $[IP_3]_c$ evoked by the stimuli when the resting level of $[IP_3]_c$ is sufficiently low (<100 nM). The possibility of saturation of the IRIS-1 signals was further investigated with IRIS-1.2, a low-affinity mutant of IRIS-1 in which lysine 249 is replaced by glutamine (K249Q). IRIS-1.2 exhibited approximately sevenfold lower affinity for IP_3 than IRIS-1 (Fig. S1 D). FRET signals observed with IRIS-1.2 revealed temporal patterns similar to those observed with IRIS-1 during Ca^{2+} oscillations evoked by mGluR5a stimulation (Fig. S1, E and F). The IRIS-1.2 signals rapidly rose after the addition of glutamate, and they remained at the elevated level and underwent fluctuations (but not baseline spikes) during Ca^{2+} oscillations. These results indicate that the IRIS-1 signals in intact cells were not saturated when the mGluR5a-expressing HeLa cells were stimulated with 100 μM glutamate. The rate of changes in IRIS-1 signals was evaluated directly by measurements of the fluorescent changes of IRIS-1 after rapid mixing with IP_3 using stopped-flow fluorescence spectrometry (see the supplemental text and Fig. S2, available at http://www.jcb.org/cgi/content/full/jcb.200512141/DC1). The analysis of the kinetics of the fluorescence changes indicates that there are two conformations of IRIS-1 with a different FRET efficiency and only IRIS-1 with a low FRET efficiency is able to bind to IP_3 (see the supplemental text). The kinetic parameters were estimated from both the kinetics data (Fig. S2 B) and the equilibrium data (Fig. S2 C) and were used to calculate the FRET changes during and after the addition of a brief pulse of IP_3. The resting level of $[IP_3]_c$ was configured to be 40 nM based on measurements in *Xenopus laevis* oocytes (Luzzi et al., 1998). Fig. S2 D shows the dynamics of the fraction of IRIS-1 with low FRET efficiency evoked by a 1-s pulse of various concentrations of IP_3 (from 200 nM to 12.8 μM). The fraction of IRIS-1 with low FRET efficiency increased more than twofold 1 s after the onset of the IP_3 pulses and returned to its basal level within 3 s after the IP_3 pulses with all concentrations applied (Fig. S2 D). The frequency of the Ca^{2+} oscillations in the IRIS-1–expressing cells stimulated with 100 μM glutamate was 36.9 ± 7.4 mHz (Fig. 3 B), and the mean duration of the interspike interval was 27.1 s. If $[IP_3]_c$ actually returns to it basal level during the period of each Ca^{2+} spike, IRIS-1 would be able to monitor it. We therefore concluded that IRIS-1 possesses a sufficient temporal property to detect $[IP_3]_c$ changes during Ca^{2+} oscillations evoked in HeLa cells.

Relationship between $[IP_3]_c$ and $[Ca^{2+}]_c$ during the rising phase of Ca^{2+} spikes

Spatiotemporal profiles of both $[Ca^{2+}]_c$ and cytosolic $[IP_3]$ at the onset of initial Ca^{2+} spikes in HeLa cells after mGluR5a stimulation were monitored with the fast acquisition equipment (see Materials and methods). Images were acquired every 246 ms.

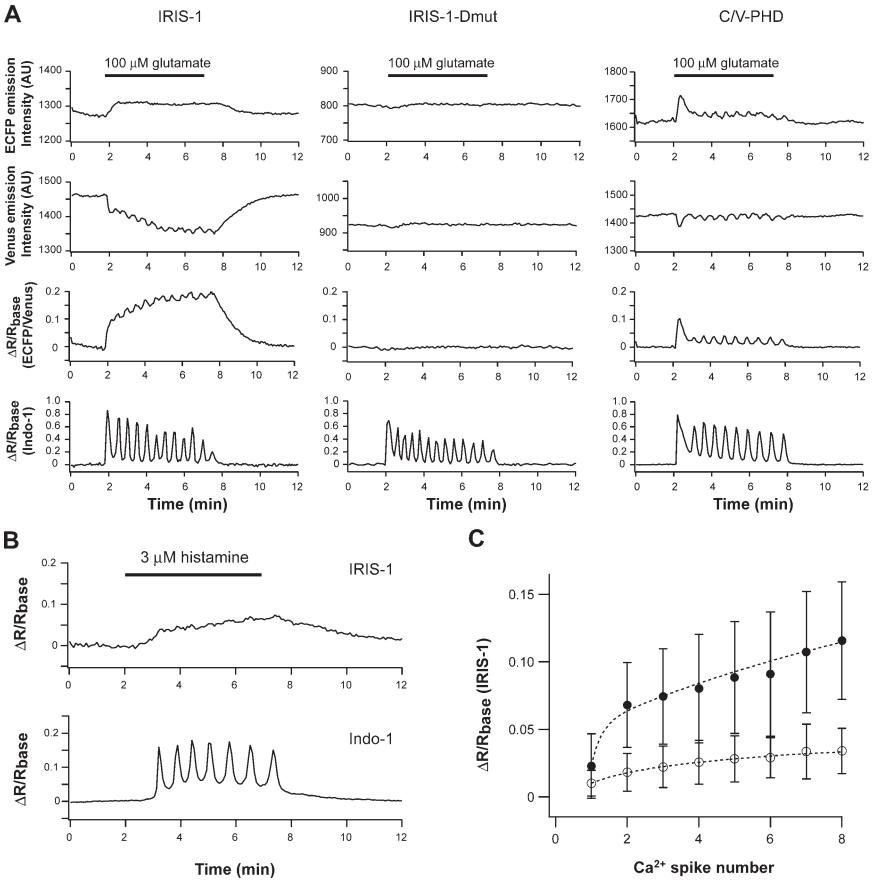

Figure 4. **IP_3 dynamics during Ca^{2+} oscillations.** (A) HeLa cells expressing mGluR5a were stimulated with 100 μM of glutamate (horizontal bars). Similar results were observed in 28 out of 29 cells (IRIS-1), 15 out of 17 cells (IRIS-1–Dmut), and 3 out of 12 cells (C/V-PHD). (B) IRIS-1–expressing HeLa cells were stimulated with 3 μM of histamine (horizontal bar). Similar results were observed in 15 cells. (C) The IP_3 concentrations at the time of the onset of each Ca^{2+} spike are shown over the Ca^{2+} spike number. Results from mGluR5a-expressing HeLa cells stimulated with 100 μM of glutamate (closed circle) and HeLa cells stimulated with 3 μM of histamine (open circle) are shown. Values are averaged for 14–24 measurements (closed circle) and 6–15 measurements (open circle). Error bars correspond to the SD.

Fig. 5 shows the spatiotemporal patterns of $[Ca^{2+}]_c$ and $[IP_3]_c$ when the first Ca^{2+} spike occurred. The rapid $[Ca^{2+}]_c$ rise occurred in HeLa cells stimulated with 100 μM glutamate with little or no pacemaker Ca^{2+} rise (Fig. 5 B). No clear initiation site of the $[Ca^{2+}]_c$ rise was detected in the cell shown (Fig. 5 A). The $[IP_3]_c$ rise was found to precede the abrupt $[Ca^{2+}]_c$ rise (Fig. 5, B and C) in 48 of 52 cells, and $[IP_3]_c$ gradually rose almost homogeneously in the cells stimulated (Fig. 5 A). The onset of the $[IP_3]_c$ rise, which was identified as an increase greater than twice the SD of the baseline signals, preceded the onset of the $[Ca^{2+}]_c$ rise by 1.11 ± 1.75 s (n = 52). The rate of $[IP_3]_c$ rise did not accelerate during the rising phase of the Ca^{2+} spike (Fig. 5, B and C, between c and e). If the regenerative IP_3 production mediated by PLC drives the rising phase of Ca^{2+} spikes, the rate of $[IP_3]_c$ rise should peak when the rate of $[Ca^{2+}]_c$ rise is at its maximum. To test this possibility, the fluorescent signals of both Indo-1 and IRIS-1 were differentiated and aligned at the time when the rate of $[Ca^{2+}]_c$ rise reached its maximum (Fig. 5, D and E). As shown in Fig. 5 E, the rate of $[IP_3]_c$ rise did not peak when the rate of $[Ca^{2+}]_c$ increase was at its maximum, indicating that the steep rise in $[Ca^{2+}]_c$ occurred without any acceleration of the $[IP_3]_c$ rise. A similar relationship was observed between $[Ca^{2+}]_c$ and $[IP_3]_c$ during the rising phases of the subsequent Ca^{2+} spikes (Fig. 6). As reported in histamine-stimulated HeLa cells (Bootman and Berridge, 1996), the shape of the first and the subsequent Ca^{2+} spikes was different in mGluR5a-expressing HeLa cells stimulated with glutamate. The subsequent spikes had more extended pacemaker activity, and the rate of the $[Ca^{2+}]_c$ rise after the pacemaker activity of the subsequent spikes was slower than that of the first spike (Fig. 6 A). As shown in Fig. 6, $[IP_3]_c$ started to increase before the onset of the pacemaker $[Ca^{2+}]_c$ rise of the second, third, and fourth Ca^{2+} spikes (filled and open arrowheads), and the $[IP_3]_c$ increase did not accelerate during the period of the rapid $[Ca^{2+}]_c$ rise of these Ca^{2+} spikes (between the thin vertical lines). The number of cells that showed $[IP_3]_c$ rises preceding $[Ca^{2+}]_c$ increases and the mean interval between the onset of the $[IP_3]_c$ rise and the onset of the $[Ca^{2+}]_c$ rise are summarized in Table S1 (available at http://www.jcb.org/cgi/content/full/jcb.200512141/DC1). These results suggest that regenerative IP_3 production does

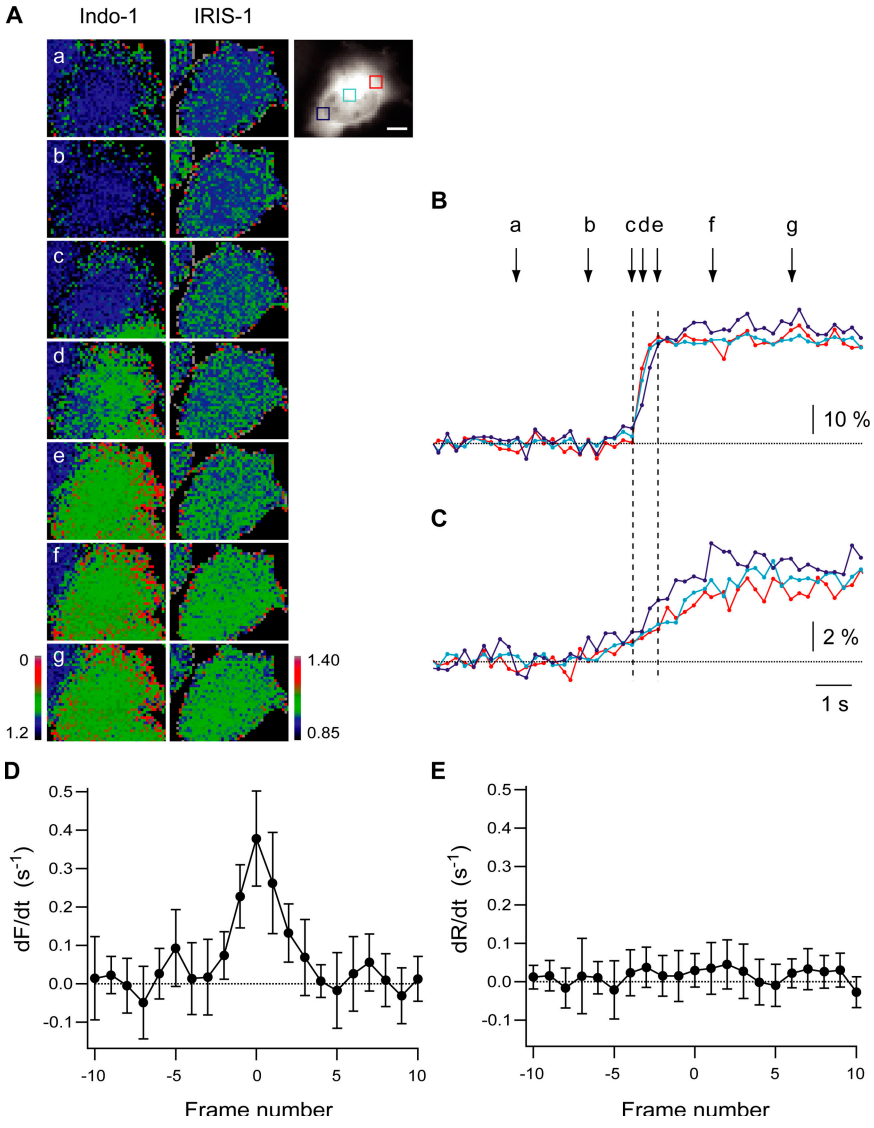

Figure 5. **IP_3 dynamics during the first Ca^{2+} spikes evoked in mGluR5a-expressing HeLa cells.** (A) Pseudocolor images of Indo-1 and IRIS-1 signals in mGluR5a-expressing HeLa cells treated with 100 μM glutamate. The fluorescent signal of Venus of IRIS-1 before the glutamate stimulation is shown as a gray-scale image. Emission at 460–490 nm (F) divided by its basal level (F_{base}) and ECFP/Venus emission ratio (R) divided by its basal level (R_{base}) are shown for Indo-1 (F/F_{base}) and IRIS-1 (R/R_{base}), respectively. Images at times a–g, which are indicated in B, are shown. Bar, 20 μm. (B and C) Time courses of emission changes of Indo-1 ($-F/F_{base}$; B) and IRIS-1 (R/R_{base}; C) during the first Ca^{2+} spike evoked by 100 μM glutamate. Signals in the area shown in the gray-scale image (A) have been plotted. Broken horizontal lines indicate baseline levels. Broken vertical lines (c and e) indicate the onset and the end of the abrupt $[Ca^{2+}]_c$ rise. (D and E) Differentiated signals of Indo-1 (D) and IRIS-1 (E) aligned by the time when the differentiated Indo-1 signal was at its maximum (frame 0). All data were collected from relatively small regions (40 × 40 pixels; 12.8 × 12.8 μm) located in the cytosol. Error bars correspond to the SD (n = 13).

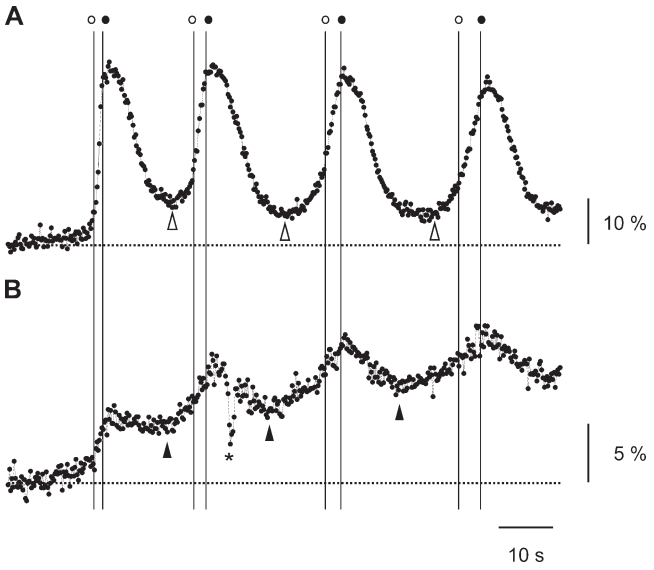

Figure 6. **IP_3 dynamics during the first and the subsequent Ca^{2+} spikes in mGluR5a-expressing HeLa cells.** Time courses of emission changes of Indo-1 ($-F/F_{base}$; A) and IRIS-1 (R/R_{base}; B) during the first four Ca^{2+} spikes evoked by 100 μM glutamate. Broken horizontal lines indicate baseline levels. Vertical lines indicate the time of the onset (open circle) and the end (closed circle) of the abrupt $[Ca^{2+}]_c$ rises. Open and closed arrowheads indicate the time of onset of the increase in the Indo-1 and IRIS-1 signals, respectively. The asterisk represents an artifact.

not drive the abrupt Ca^{2+} increase of either the first or the subsequent Ca^{2+} spikes in mGluR5a-stimulated HeLa cells.

Ca^{2+}-dependent IP_3 production in HeLa cells

Ca^{2+}-dependent stimulation of PLC activity has been proposed to be a positive-feedback element that causes the steep rising phase of Ca^{2+} spikes (Meyer and Stryer, 1988). As shown in Figs. 5 and 6, however, the rapid increase in $[Ca^{2+}]_c$ in the rising phase of Ca^{2+} spikes was unaccompanied by any acceleration of the $[IP_3]_c$ rise. To evaluate the component of the Ca^{2+}-dependent IP_3 production in HeLa cells, $[IP_3]_c$ was monitored in the cells in which $[Ca^{2+}]_c$ increased without activation of G protein–coupled receptors. HeLa cells were treated with 1 μM thapsigargin for 5 min to deplete intracellular stores and then exposed to 2 mM Ca^{2+}. In these cells, a $[IP_3]_c$ increase that exceeded twice the SD of the baseline signal was detected with a much greater delay (66.6 ± 13.6 s; $n = 9$) than the onset of the $[Ca^{2+}]_c$ increase mediated by capacitative Ca^{2+} entry (Fig. 7 A). IP_3 signals were well fitted with a monoexponential function having a time constant of 85.7 ± 25.1 s ($n = 10$). Histamine stimulation alone in the absence of extracellular Ca^{2+} induced a rapid but small increase in $[IP_3]_c$ (Fig. 7 B). When thapsigargin-treated cells were stimulated with 3 μM histamine in the presence of 2 mM extracellular Ca^{2+}, $[IP_3]_c$ increased in a complex pattern consisting of a rapid transient increase (Fig. 7 B, arrowheads) followed by a slow sustained increase (Fig. 7 C). The amplitude of the initial rapid transient was far below the maximal IP_3 concentration observed at the end of the stimulation (Fig. 7 C). The rapid transient increase in $[IP_3]_c$ was never observed in the thapsigargin-treated cells stimulated with histamine alone ($n = 14$; Fig. 7 B) or with extracellular Ca^{2+} alone ($n = 19$; Fig. 7 A). There were no differences in rate of Ca^{2+} increase and maximal Ca^{2+} concentration reached between the cells stimulated with extracellular Ca^{2+} alone (Fig. 7 A) and the cells stimulated with histamine in the presence of extracellular Ca^{2+} (Fig. 7 C). Similar temporal patterns of $[Ca^{2+}]_c$ were obtained with Fura-4F ($K_d = 770$ nM; unpublished data), indicating that Indo-1 was not saturated under the conditions used. These results indicate

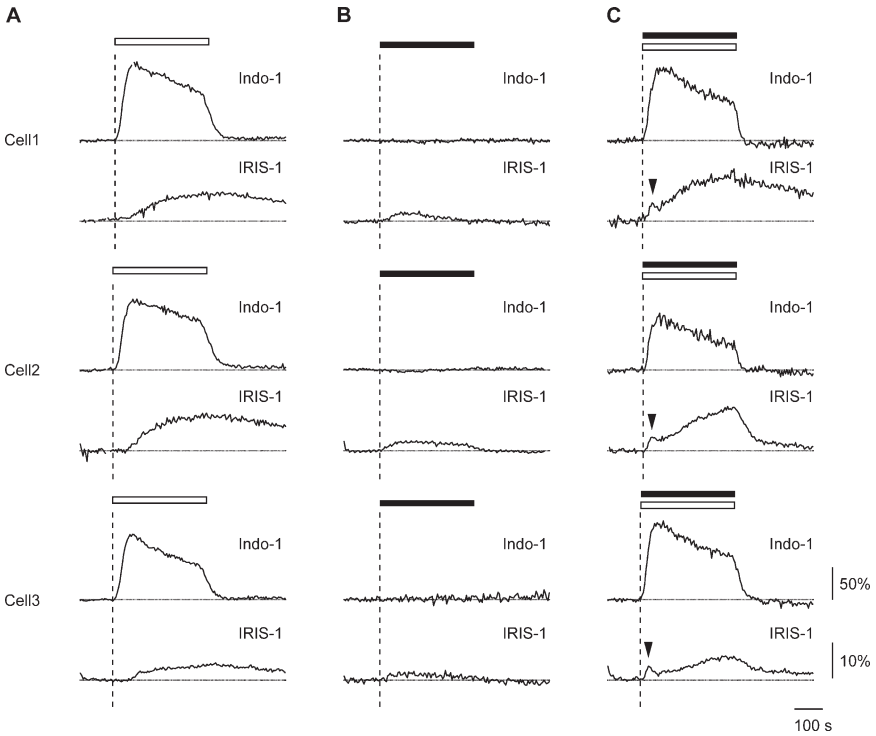

Figure 7. **Ca^{2+}-dependent component of IP_3 production in HeLa cells.** Cells were treated with 1 μM thapsigargin in the absence of extracellular Ca^{2+} for 5 min and then exposed to 2 mM extracellular Ca^{2+} (A, open horizontal bar), 3 μM histamine (B, closed horizontal bar), or 3 μM histamine plus 2 mM extracellular Ca^{2+} (C, open and closed horizontal bars). Indo-1 signals ($\Delta R/R_{base}$; top) and IRIS-1 signals ($\Delta R/R_{base}$; bottom) of three cells are shown. Arrowheads point to transient $[IP_3]_c$ increases. Broken horizontal lines indicate the baseline level of Indo-1 and IRIS-1 signals. Broken vertical lines indicate the time of the onset of stimulation. Images were acquired every 4 s.

that (1) the cytosolic Ca^{2+} increase itself induces IP_3 production in HeLa cells, but the process is relatively slow compared with agonist stimulation–evoked IP_3 production, and (2) receptor activation and the $[Ca^{2+}]_c$ increase synergistically induce the rapid, transient IP_3 production in HeLa cells, but the amplitude of the IP_3 transient is relatively small even when $[Ca^{2+}]_c$ is persistently elevated.

Discussion

We developed cytosolic IP_3 sensors based on the IP_3 binding domain of mouse IP_3R1 and used them to analyze the mechanism that generates $[Ca^{2+}]_c$ oscillations. Nonexcitable human HeLa carcinoma cells were chosen to measure cytosolic IP_3 dynamics because they have been used by several groups as a model system to study hormone-evoked Ca^{2+} signals. We had already developed the high-affinity IP_3 binding protein based on the IP_3 binding domain of mouse IP_3R1, the IP_3 sponge, to chelate cytosolic IP_3 (Uchiyama et al., 2002), and found that introduction of the IP_3 sponge into living cells significantly inhibits or completely suppresses stimulus-evoked intracellular Ca^{2+} increases (Iwasaki et al., 2002; Uchiyama et al., 2002). The challenge was to develop low IP_3 binding affinity IP_3 sensors with a sufficient signal-to-noise ratio to monitor the physiological dynamics of cytosolic IP_3 without serious impairment of Ca^{2+} signals. We created >300 recombinant proteins and found that IRIS-1 exhibited a 25.1 ± 8.0% FRET ratio change upon the addition of an excess amount of IP_3 with a K_d value of 549 ± 62 nM in cell lysates (Fig. 1) and did not significantly alter the Ca^{2+} oscillation frequency or rate of decrease in individual Ca^{2+} spikes in mGluR5a-stimulated HeLa cells (Fig. 3). We used mGluR5a as a surface receptor that is linked with phosphoinositide hydrolysis, as the receptor has been used to investigate the mechanism of generation of Ca^{2+} oscillations (Kawabata et al., 1996) and to measure IP_3 dynamics with GFP-tagged PHD (Nash et al., 2002). We used IRIS-1 to simultaneously monitor the spatiotemporal dynamics of both $[Ca^{2+}]_c$ and $[IP_3]_c$ in single living cells and investigated the mechanism underlying the generation of Ca^{2+} oscillations. In mGluR5a-stimulated HeLa cells, $[IP_3]_c$ started to increase at a relatively constant rate before the pacemaker $[Ca^{2+}]_c$ rise and the subsequent abrupt $[Ca^{2+}]_c$ rise did not accelerate the rate of $[IP_3]_c$ rise (Figs. 5 and 6). $[IP_3]_c$ did not return to its basal level during the interval between Ca^{2+} spikes and, as a result, IP_3 gradually accumulated in the cytosol with little (Fig. 4 A and Fig. 6) or no detectable (Fig. 4 B) fluctuations when repeated Ca^{2+} spikes occurred in the continuous presence of the stimulus. Each Ca^{2+} spike seemed to be triggered at a different concentration of $[IP_3]_c$ (Fig. 4 C and Fig. 6), contradicting the findings by other investigators that Ca^{2+} spikes are triggered at a critical $[Ca^{2+}]_c$ (Iino et al., 1993). Our results indicate that (1) Ca^{2+}-induced regenerative IP_3 production is not a driving force of the abrupt upstroke of Ca^{2+} spikes, (2) the apparent IP_3 sensitivity for generation of Ca^{2+} spikes progressively decreases during Ca^{2+} oscillations, and (3) the clearance of IP_3 in the cytosol of living cells is slower than the decrease of cytosolic Ca^{2+}.

Positive-feedback element that drives the steep rising phase of Ca^{2+} spikes

Meyer and Stryer (1988) proposed that cytosolic Ca^{2+} and IP_3 are a pair of reciprocally coupled messengers based on evidence that IP_3 induces cytosolic Ca^{2+} increase by triggering Ca^{2+} release from intracellular Ca^{2+} stores and that Ca^{2+} enhances IP_3 production by activating PLC. Their model predicts that the cooperative opening of IP_3R by the binding of multiple IP_3 molecules and positive-feedback regulation of PLC by cytosolic Ca^{2+} lead to the bistability of the system (Meyer and Stryer, 1988) and that IP_3 spikes in synchrony with Ca^{2+} spikes (we use "spike" to mean a threshold phenomenon characterized by an explosive rise and constant amplitude independent of stimulus intensity; Meyer and Stryer, 1988, 1991). We used the cytosolic IP_3 sensor IRIS-1 to directly test the cross-coupling hypothesis in living HeLa cells and found that no IP_3 spikes were detected during Ca^{2+} oscillations, according to the aforementioned definition, because the IRIS-1 signals did not exhibit an explosive rise during the rising phase of Ca^{2+} spikes (Figs. 5 and 6), and even when fluctuations were detected the absolute value of the peak level of fluctuations in IRIS-1 signals was not constant during Ca^{2+} oscillations evoked by mGluR5a stimulation (Figs. 4 and 6). The dynamic range of the IRIS-1 signals seems to be wider than the dynamic range of $[IP_3]_c$ changes evoked by extracellular stimuli (Fig. S1 C), and the sevenfold lower IP_3 binding affinity mutant of IRIS-1, IRIS-1.2, also failed to detect IP_3 spikes (Fig. S1 E). The reaction of IRIS-1 is thought to be fast enough to detect $[IP_3]_c$ changes during Ca^{2+} oscillations in mGluR5a-expressing HeLa cells, which exhibited 36.9 ± 7.4 mHz of Ca^{2+} oscillations (Fig. S2 D). Thus, the failure to detect IP_3 spikes was not due to inability because of either the dynamic range or time resolution of IRIS-1. Fast acquisition of both Ca^{2+} and IP_3 signals revealed that $[IP_3]_c$ started to increase before the pacemaker rise in $[Ca^{2+}]_c$, and the abrupt increase in $[Ca^{2+}]_c$, which forms the rising phase of Ca^{2+} spikes, was not accompanied by a detectable acceleration in the $[IP_3]_c$ increase (Figs. 5 and 6). The cytosolic Ca^{2+} increases actually induced IP_3 production in HeLa cells without G protein–coupled receptor activation (Fig. 7 A), but it was a relatively slow process compared with the IP_3 production evoked by histamine (Fig. 7 B). Receptor activation and $[Ca^{2+}]_c$ increases have a synergistic effect on IP_3 production, but it was not sufficiently strong to generate IP_3 spikes even when $[Ca^{2+}]_c$ was persistently elevated (Fig. 7 C). Although we cannot completely exclude the possibility that the local rapid rise in $[IP_3]_c$ contributes to the generation of the rising phase of Ca^{2+} spikes, we used relatively small regions (Fig. 5 A), not the entire cytosol, to analyze the relationship between $[Ca^{2+}]_c$ and $[IP_3]_c$ and found that any acceleration in the $[IP_3]_c$ increase was not detected in the region in which $[Ca^{2+}]_c$ rose abruptly (Fig. 5, C and E). We therefore concluded that IP_3 spikes do not occur during Ca^{2+} oscillations in HeLa cells and that the positive-feedback regulation of PLC by cytosolic Ca^{2+} is not a prime mechanism for the generation of the upstroke of Ca^{2+} spikes.

What is the positive-feedback element that drives the rising phase of Ca^{2+} spikes? One plausible mechanism is Ca^{2+}-induced Ca^{2+} release (CICR) mediated by IP_3R. IP_3R is activated

by cytosolic Ca^{2+}, and positive-feedback regulation by cytosolic Ca^{2+} enables the Ca^{2+} released by one receptor to excite its neighbors, thereby igniting a regenerative Ca^{2+} wave. However, we did not test the CICR hypothesis in the present study. The CICR hypothesis needs to be evaluated more directly under native conditions in future studies.

Mechanisms of initiation of the steep rising phase of Ca^{2+} spikes

We found that $[IP_3]_c$ started to increase before the pacemaker rise in $[Ca^{2+}]_c$ and that the subsequent steep rise in $[Ca^{2+}]_c$ was unaccompanied by any acceleration in the $[IP_3]_c$ increase (Figs. 5 and 6). The individual abrupt $[Ca^{2+}]_c$ rises of at least the first eight Ca^{2+} spikes were initiated at different concentrations of $[IP_3]_c$ (Fig. 4 C), and the Ca^{2+} spikes of mGluR5a-expressing cells stimulated with 100 μM glutamate and cells stimulated with 3 μM histamine were triggered at different IP_3 concentrations (Fig. 4 C). These results indicate that a constant threshold $[IP_3]_c$ is not involved in the initiation of the steep Ca^{2+} rise in HeLa cells. What is the actual trigger for generation of the rapid upstroke of Ca^{2+} spikes? Numerous observations have shown that elevation of $[IP_3]_c$ to submaximal levels causes only a transient, partial release of Ca^{2+}, whereas further increments of $[IP_3]_c$ evoke an additional transient Ca^{2+} release (Muallem et al., 1989; Taylor and Potter, 1990; Bootman et al., 1992; Ferris et al., 1992; Hirota et al., 1995; Yao et al., 1995). Subsequent elevations of $[IP_3]_c$ yielded the same degree of Ca^{2+} release as the first $[IP_3]_c$ elevation, and the retention of responsiveness has been called "incremental detection" (Meyer and Stryer, 1990). However, because we did not detect rapid increments in $[IP_3]_c$ when the abrupt $[Ca^{2+}]_c$ rises were triggered (Fig. 5, D and E), IP_3-sensitive Ca^{2+} stores did not respond to the rate of $[IP_3]_c$ increase in the cells examined. A time-dependent decrease in the IP_3 binding affinity of IP_3-gated Ca^{2+} release channels and/or multiple Ca^{2+} stores with different levels of IP_3 sensitivity could account for this phenomenon. Ca^{2+} influx across plasma membranes might be involved in the initiation of repetitive spikes (Sneyd et al., 2004). Further analysis is required for the elucidation of the Ca^{2+} spike initiation mechanism.

IP_3 metabolism in living cells

The mechanism underlying the generation of Ca^{2+} oscillations has been extensively investigated using various theoretical models. What kind of uncertainty is involved in such analyses? To address this issue, we tried to reproduce the experimental measurements of both IP_3 and Ca^{2+} dynamics using a model based on previously reported models that incorporate the biphasic cytosolic Ca^{2+} dependency of IP_3R and Ca^{2+} feedback on the production of IP_3 (Meyer and Stryer, 1991; De Young and Keizer, 1992; Fig. S3, available at http://www.jcb.org/cgi/content/full/jcb.200512141/DC1). The model exhibited sharp Ca^{2+} oscillations accompanied by IP_3 oscillations (Fig. S3, A and B) with the original parameters (Table S2; De Young and Keizer, 1992). When we compared the calculated trace of cytosolic IP_3 with the experimental measurements (Fig. 4), the $[IP_3]_c$ change predicted by the model was obviously too fast. We found that an ~60-fold decrease in the rate of IP_3 production (Fig. S3 E and Table S2) and a 30-fold decrease in the rate of IP_3 degradation (Fig. S3 F and Table S2) produced reasonable $[IP_3]_c$ changes (Fig. S3 C) accompanied by repetitive Ca^{2+} spikes (Fig. S3 D). The calculated Ca^{2+} dynamics (Fig. S3 D), however, were significantly different from the experimentally observed Ca^{2+} dynamics (Fig. 4) in terms of frequency and latency. Because the apparent IP_3 sensitivity for the generation of Ca^{2+} spikes progressively decreases during Ca^{2+} oscillations (Fig. 4 C), this property must be incorporated into the IP_3R model. It is clear that the actual IP_3 metabolism in living cells is slower than previously estimated (Meyer and Stryer, 1991; De Young and Keizer, 1992). A similar conclusion was obtained from the estimation of the lifetime of IP_3 in N1E-115 neuroblastoma cells (Wang et al., 1995).

Allbritton et al. (1992) proposed that Ca^{2+} is a local messenger, whereas IP_3 is a global messenger based on their diffusion constants estimated in isolated cytosol. We propose that Ca^{2+} is a fast messenger and IP_3 a slow messenger, based on the evidence that the concentration change of cytosolic IP_3 is slower than that of Ca^{2+} in living cells. IP_3R functions as a pulse generator in the signal transduction cascade that translates the information from the slow IP_3 signal to the fast Ca^{2+} signal. Elucidation of the encoding algorithm of this signal conversion is the next challenge in terms of better understanding the molecular basis of Ca^{2+} signaling.

Materials and methods

Materials

An anti-GFP antibody and an anti-mGluR5 antibody were purchased from MBL International Corporation and Upstate Biotechnology, respectively.

Gene construction

The IP_3 binding core cDNA was obtained by PCR from pBact-ST-neoB-C1 (Furuichi et al., 1989; Miyawaki et al., 1990). Venus (Nagai et al., 2002) and ECFP cDNAs were fused to the 5′ and the 3′ end, respectively, of the IP_3 binding domain to produce IRIS proteins. Mutations of T267A and K508Q or K249Q were introduced as described elsewhere (Sawano and Miyawaki, 2000) to create an IP_3 binding–deficient mutant and a low IP_3 binding–affinity mutant, respectively. IP_3 sensor cDNAs were cloned in BamHI and XhoI sites of pcDNA3.1 zeo(+) (Invitrogen) that contains 6× Histidine tag (Fig. 1 A) in NheI to HindIII site for the expression in mammalian cells. The multicloning site of pcDNA3.1 zeo(+) was amplified by PCR and cloned into SalI site of pFastBacI (Invitrogen). IRIS-1 and IRIS-1–Dmut were digested by NheI and XhoI from pcDNA3.1 zeo(+) and inserted to the modified pFastBacI for the expression in Sf9 cells. Venus or ECFP cDNA was fused to 5′ end of cDNA corresponding to amino acid residues 11–140 of rat PLCδ1 to create V-PHD (provided by M. Hattori, Nagoya City University, Aichi, Japan) and C-PHD, respectively. The resulting cDNAs were cloned in pcDNA3.1 zeo(+). Rat mGluR5a cDNA inserted into pME18S (Kawabata et al., 1996) was a gift from S. Nakanishi (Osaka Bioscience Institute, Osaka, Japan).

Expression, purification, and characterization in vitro

In vitro characterization of IRIS proteins were performed by using lysates prepared from COS7 or Sf9 cells expressing IRIS proteins and IRIS proteins purified from Sf9 cells. COS7 cells expressing IRIS proteins were lysed with the solution containing 10 mM Hepes, pH 7.4, 100 mM NaCl, 1 mM EDTA, 1 mM 2-mercaptoethanol, and 0.5% NP-40. His-tagged IRIS-1 and IRIS-1–Dmut proteins were expressed by means of Sf9 baculovirus–expressing system (Invitrogen) and were purified as follows. Sf9 cells were suspended in homogenization solution containing 10 mM Hepes, pH 7.8, 100 mM NaCl, 5 mM 2-mercaptoethanol, 0.1% NP-40, and proteinase inhibitors (0.1 mM PMSF, 10 μM Leupeptin, 10 μM Pepstatin A, and 10 μM E60) and were homogenized at 1,000 rpm for 10 strokes at 4°C. Homogenates were applied to Probond resin (Invitrogen), and His-tagged proteins were eluted with 300 mM imidazole. Proteins were then dialyzed for 30 min against the solution containing 10 mM Hepes, pH 7.4, and 100 mM KCl.

The dialyzed proteins were loaded to HiTrap heparin columns and eluted with the high KCl solution containing 10 mM Hepes, pH 7.4, and 250 mM KCl. Proteins were diluted by adding two volumes of the solution containing 10 mM Hepes, pH 7.4, and 100 mM KCl and concentrated with centrifugal filter devices (30,000 MWCO; Amicon Ultra 15 [Millipore]). For the evaluation of the rate of changes in IRIS-1 signals, IRIS-1–expressing Sf9 cells were suspended in 10 mM Hepes, pH 7.4, 100 mM NaCl, 1 mM EDTA, 1 mM 2-mercaptoethanol, 0.01% NP-40, and proteinase inhibitors and were homogenized at 1,000 rpm for 10 strokes at 4°C. The homogenates were centrifuged at 20,000 *g* for 30 min, and the supernatants were used for stopped-flow fluorescent measurements. The number of IRIS-1 molecules in the supernatants was quantified by the equilibrium IP_3 binding analysis using $[^3H]IP_3$ as described previously (Iwai et al., 2005). IRIS signals were measured with a spectrofluorometer (FP-750; Jasco).

Imaging

IRIS cDNAs inserted in pcDNA3.1 zeo(+) were transfected into HeLa cells with transfection reagents (TransIT; Mirus). After 12–36 h, cells were used for imaging. After loading the cells with 5 μM Indo-1 AM (DOJINDO), imaging was performed under the constant flow (2 ml/min) of the balanced salt solution containing 20 mM Hepes, pH 7.4, 115 mM NaCl, 5.4 mM KCl, 1 mM $MgCl_2$, 2 mM $CaCl_2$, and 10 mM glucose as an imaging media at 37°C. Imaging was performed at 37°C through an inverted microscope (IX-71 or IX-81; Olympus) with a cooled charge-coupled device camera (ORCA-ER; Hamamatsu Photonics) and a 40× (NA 1.35) objective. A 333–348-nm excitation filter and pair of 420–440- and 460–510-nm emission filters and a 425–445-nm excitation and pair of 460–510-nm (cyan) and 525–565-nm (yellow) emission filters were used for fluorochromes (Indo-1 and IRIS, respectively). Beam-splitter mirrors (400 and 450 nm) were alternately inserted into the light path for Indo-1 and IRIS, respectively. Images were acquired at 0.25 Hz, with an exposure time of 100 or 150 ms. For the fast acquisition (4.07 Hz) of fluorescent images of IRIS-1 and Indo-1, an emission splitter (W-view; Hamamatsu Photonics) was used with a fast light source exchanger (DG-4; Sutter Instrument Co.) on the IX71 inverted microscope. Sequential excitation of IRIS-1 and Indo-1 was performed by using a 450-nm dichroic mirror and two excitation filters (a 425–445-nm filter for IRIS-1 and a 333–348-nm filter for Indo-1). Dual emission at 460–490 nm (for IRIS-1 and Indo-1) and >520 nm (for IRIS-1) split with a 460–490-nm filter, a long-path 520-nm barrier filter, and two 505-nm dichroic mirrors equipped in W-view. Images were acquired at 4.07 Hz, with an exposure time of 100 or 150 ms. Acquisition was performed with the custom software TI Workbench (written by T. Inoue). Off-line analysis was performed with TI Workbench combined with Igor Pro software (WaveMetrics). Spectral analysis of Ca^{2+} oscillations was performed as described previously (Uhlen, 2004).

Stopped-flow fluorescent measurement

The change in the intensity of Venus fluorescence (525 ± 20 nm) of IRIS-1 after the addition of various concentrations of IP_3 was monitored using the FP-750 spectrofluorometer with a stopped-flow rapid mixing accessory (RX2000; Applied Photophysics). The IRIS-1–containing supernatants (final 2.5 nM of IRIS-1) were mixed with a 24-fold–excess volume of 10 mM Hepes, pH 7.4, 100 mM NaCl, 1 mM EDTA, 1 mM 2-mercaptoethanol, and 0.01% NP-40 containing various concentrations of IP_3 at 25°C, and the change of the intensity of Venus fluorescence of IRIS-1 excited at 440 ± 20 nm was monitored at 1,000 Hz. At least 10 traces were averaged and were used for the nonlinear regression analysis with Igor Pro software. The IP_3 dependency of FRET changes of IRIS-1 at equilibrium was monitored using the same batches of the supernatants as used for the kinetic measurements with a 1-cm cuvette and the FP-750 spectrofluorometer.

Online supplemental material

Fig. S1 shows effects of PLC inhibitors on emission changes of IRIS-1 elicited by 10 μM of histamine and evaluation of IRIS-1 signals observed in living HeLa cells. Fig. S2 shows the rate of reaction of IRIS-1. Fig. S3 shows simulation of IP_3 and Ca^{2+} dynamics. Table S1 shows numbers of cells that showed $[IP_3]_c$ rises preceding $[Ca^{2+}]_c$ increases, the mean intervals between the onset of $[IP_3]_c$ rises, and the onset of $[Ca^{2+}]_c$ rises. Table S2 shows the parameters used to calculate IP_3 and Ca^{2+} dynamics. The supplemental text shows evaluation of the effect of the rate of FRET changes of IRIS-1 upon IP_3 binding. Online supplemental material is available at http://www.jcb.org/cgi/content/full/jcb.200512141/DC1.

We thank Drs. Takeshi Nakamura, Takeharu Nagai, Masaki Sano, Toshio Aoyagi, Hideki Nakamura, Yoko Tateishi, and Sachiko Ishida for fruitful discussions and Ms. Naoko Ogawa and Miwako Iwai for excellent technical support.

This work was supported by The 21st Century Center of Excellence program, the Center for Integrated Brain Medical Science, and grants from the Ministry of Education, Culture, Sports, Science and Technology of Japan to T. Matsu-ura (18770144), T. Michikawa (17017013 and 17570128), and T. Inoue and K. Mikoshiba (15100006); the Ministry of Health, Labor and Welfare to T. Inoue; and the Moritani Scholarship Foundation to T. Michikawa.

Submitted: 27 December 2005
Accepted: 3 May 2006

References

Allbritton, N.L., T. Meyer, and L. Stryer. 1992. Range of messenger action of calcium ion and inositol 1,4,5-trisphosphate. *Science.* 258:1812–1815.

Berridge, M.J. 1988. Inositol trisphosphate-induced membrane potential oscillations in *Xenopus* oocytes. *J. Physiol.* 403:589–599.

Berridge, M.J., and G. Dupont. 1994. Spatial and temporal signalling by calcium. *Curr. Opin. Cell Biol.* 6:267–274.

Berridge, M.J., P. Lipp, and M.D. Bootman. 2000. The versatility and universality of calcium signalling. *Nat. Rev. Mol. Cell Biol.* 1:11–21.

Bootman, M.D., and M.J. Berridge. 1996. Subcellular Ca^{2+} signals underlying waves and graded responses in HeLa cells. *Curr. Biol.* 6:855–865.

Bootman, M.D., M.J. Berridge, and C.W. Taylor. 1992. All-or-nothing Ca^{2+} mobilization from the intracellular stores of single histamine-stimulated HeLa cells. *J. Physiol.* 450:163–178.

Bosanac, I., J.R. Alattia, T.K. Mal, J. Chan, S. Talarico, F.K. Tong, K.I. Tong, F. Yoshikawa, T. Furuichi, M. Iwai, et al. 2002. Structure of the inositol 1,4,5-trisphosphate receptor binding core in complex with its ligand. *Nature.* 420:696–700.

Cobbold, P.H., A. Sanchez-Bueno, and C.J. Dixon. 1991. The hepatocyte calcium oscillator. *Cell Calcium.* 12:87–95.

De Young, G.W., and J. Keizer. 1992. A single-pool inositol 1,4,5-trisphosphate-receptor-based model for agonist-stimulated oscillations in Ca^{2+} concentration. *Proc. Natl. Acad. Sci. USA.* 89:9895–9899.

Dupont, G., M.J. Berridge, and A. Goldbeter. 1991. Signal-induced Ca^{2+} oscillations: properties of a model based on Ca^{2+}-induced Ca^{2+} release. *Cell Calcium.* 12:73–85.

Ferris, C.D., A.M. Cameron, R.L. Huganir, and S.H. Snyder. 1992. Quantal calcium release by purified reconstituted inositol 1,4,5-trisphosphate receptors. *Nature.* 356:350–352.

Furuichi, T., S. Yoshikawa, A. Miyawaki, K. Wada, N. Maeda, and K. Mikoshiba. 1989. Primary structure and functional expression of the inositol 1,4,5-trisphosphate-binding protein P_{400}. *Nature.* 342:32–38.

Hajnoczky, G., and A.P. Thomas. 1997. Minimal requirements for calcium oscillations driven by the IP_3 receptor. *EMBO J.* 16:3533–3543.

Harootunian, A.T., J.P. Kao, S. Paranjape, and R.Y. Tsien. 1991. Generation of calcium oscillations in fibroblasts by positive feedback between calcium and IP_3. *Science.* 251:75–78.

Hirose, K., S. Kadowaki, M. Tanabe, H. Takeshima, and M. Iino. 1999. Spatiotemporal dynamics of inositol 1,4,5-trisphosphate that underlies complex Ca^{2+} mobilization patterns. *Science.* 284:1527–1530.

Hirota, J., T. Michikawa, A. Miyawaki, T. Furuichi, I. Okura, and K. Mikoshiba. 1995. Kinetics of calcium release by immunoaffinity-purified inositol 1,4,5-trisphosphate receptor in reconstituted lipid vesicles. *J. Biol. Chem.* 270:19046–19051.

Iino, M. 1990. Biphasic Ca^{2+} dependence of inositol 1,4,5-trisphosphate-induced Ca release in smooth muscle cells of the guinea pig taenia caeci. *J. Gen. Physiol.* 95:1103–1122.

Iino, M., T. Yamazawa, Y. Miyashita, M. Endo, and H. Kasai. 1993. Critical intracellular Ca^{2+} concentration for all-or-none Ca^{2+} spiking in single smooth muscle cells. *EMBO J.* 12:5287–5291.

Irvine, R. 2004. Inositol lipids: to PHix or not to PHix? *Curr. Biol.* 14:R308–R310.

Iwai, M., Y. Tateishi, M. Hattori, A. Mizutani, T. Nakamura, A. Futatsugi, T. Inoue, T. Furuichi, T. Michikawa, and K. Mikoshiba. 2005. Molecular cloning of mouse type 2 and type 3 inositol 1,4,5-trisphosphate receptors and identification of a novel type 2 receptor splice variant. *J. Biol. Chem.* 280:10305–10317.

Iwasaki, H., K. Chiba, T. Uchiyama, F. Yoshikawa, F. Suzuki, M. Ikeda, T. Furuichi, and K. Mikoshiba. 2002. Molecular characterization of the starfish inositol 1,4,5-trisphosphate receptor and its role during oocyte maturation and fertilization. *J. Biol. Chem.* 277:2763–2772.

Jacob, R., J.E. Merritt, T.J. Hallam, and T.J. Rink. 1988. Repetitive spikes in cytoplasmic calcium evoked by histamine in human endothelial cells. *Nature.* 335:40–45.

Kawabata, S., R. Tsutsumi, A. Kohara, T. Yamaguchi, S. Nakanishi, and M. Okada. 1996. Control of calcium oscillations by phosphorylation of metabotropic glutamate receptors. *Nature.* 383:89–92.

Lechleiter, J., S. Girard, E. Peralta, and D. Clapham. 1991. Spiral calcium wave propagation and annihilation in *Xenopus laevis* oocytes. *Science.* 252:123–126.

Luzzi, V., C.E. Sims, J.S. Soughayer, and N.L. Allbritton. 1998. The physiologic concentration of inositol 1,4,5-trisphosphate in the oocytes of *Xenopus laevis*. *J. Biol. Chem.* 273:28657–28662.

Meyer, T., and L. Stryer. 1988. Molecular model for receptor-stimulated calcium spiking. *Proc. Natl. Acad. Sci. USA.* 85:5051–5055.

Meyer, T., and L. Stryer. 1990. Transient calcium release induced by successive increments of inositol 1,4,5-trisphosphate. *Proc. Natl. Acad. Sci. USA.* 87:3841–3845.

Meyer, T., and L. Stryer. 1991. Calcium spiking. *Annu. Rev. Biophys. Biophys. Chem.* 20:153–174.

Michikawa, T., J. Hirota, S. Kawano, M. Hiraoka, M. Yamada, T. Furuichi, and K. Mikoshiba. 1999. Calmodulin mediates calcium-dependent inactivation of the cerebellar type 1 inositol 1,4,5-trisphosphate receptor. *Neuron.* 23:799–808.

Miyawaki, A., T. Furuichi, N. Maeda, and K. Mikoshiba. 1990. Expressed cerebellar-type inositol 1,4,5-trisphosphate receptor, P_{400}, has calcium release activity in a fibroblast L cell line. *Neuron.* 5:11–18.

Miyawaki, A., T. Furuichi, Y. Ryou, S. Yoshikawa, T. Nakagawa, T. Saitoh, and K. Mikoshiba. 1991. Structure-function relationships of the mouse inositol 1,4,5-trisphosphate receptor. *Proc. Natl. Acad. Sci. USA.* 88:4911–4915.

Muallem, S., S.J. Pandol, and T.G. Beeker. 1989. Hormone-evoked calcium release from intracellular stores is a quantal process. *J. Biol. Chem.* 264:205–212.

Nagai, T., K. Ibata, E.S. Park, M. Kubota, K. Mikoshiba, and A. Miyawaki. 2002. A variant of yellow fluorescent protein with fast and efficient maturation for cell-biological applications. *Nat. Biotechnol.* 20:87–90.

Nash, M.S., M.J. Schell, P.J. Atkinson, N.R. Johnston, S.R. Nahorski, and R.A. Challiss. 2002. Determinants of metabotropic glutamate receptor-5-mediated Ca^{2+} and inositol 1,4,5-trisphosphate oscillation frequency. Receptor density versus agonist concentration. *J. Biol. Chem.* 277:35947–35960.

Osipchuk, Y.V., M. Wakui, D.I. Yule, D.V. Gallacher, and O.H. Petersen. 1990. Cytoplasmic Ca^{2+} oscillations evoked by receptor stimulation, G-protein activation, internal application of inositol trisphosphate or Ca^{2+}: simultaneous microfluorimetry and Ca^{2+} dependent Cl^- current recording in single pancreatic acinar cells. *EMBO J.* 9:697–704.

Prentki, M., M.C. Glennon, A.P. Thomas, R.L. Morris, F.M. Matschinsky, and B.E. Corkey. 1988. Cell-specific patterns of oscillating free Ca^{2+} in carbamylcholine-stimulated insulinoma cells. *J. Biol. Chem.* 263:11044–11047.

Rebecchi, M.J., and S.N. Pentyala. 2000. Structure, function, and control of phosphoinositide-specific phospholipase C. *Physiol. Rev.* 80:1291–1335.

Remus, T.P., A.V. Zima, J. Bossuyt, D.J. Bare, J.L. Martin, L.A. Blatter, D.M. Bers, and G.A. Mignery. 2006. Biosensors to measure inositol 1,4,5-trisphosphate concentration in living cells with spatiotemporal resolution. *J. Biol. Chem.* 281:608–616.

Sato, M., Y. Ueda, M. Shibuya, and Y. Umezawa. 2005. Locating inositol 1,4,5-trisphosphate in the nucleus and neuronal dendrites with genetically encoded fluorescent indicators. *Anal. Chem.* 77:4751–4758.

Sawano, A., and A. Miyawaki. 2000. Directed evolution of green fluorescent protein by a new versatile PCR strategy for site-directed and semi-random mutagenesis. *Nucleic Acids Res.* 28:E78.

Sneyd, J., K. Tsaneva-Atanasova, D.I. Yule, J.L. Thompson, and T.J. Shuttleworth. 2004. Control of calcium oscillations by membrane fluxes. *Proc. Natl. Acad. Sci. USA.* 101:1392–1396.

Tanimura, A., A. Nezu, T. Morita, R.J. Turner, and Y. Tojyo. 2004. Fluorescent biosensor for quantitative real-time measurements of inositol 1,4,5-trisphosphate in single living cells. *J. Biol. Chem.* 279:38095–38098.

Taylor, C.W., and B.V. Potter. 1990. The size of inositol 1,4,5-trisphosphate-sensitive Ca^{2+} stores depends on inositol 1,4,5-trisphosphate concentration. *Biochem. J.* 266:189–194.

Thomas, A.P., D.C. Renard, and T.A. Rooney. 1991. Spatial and temporal organization of calcium signalling in hepatocytes. *Cell Calcium.* 12:111–126.

Uchiyama, T., F. Yoshikawa, A. Hishida, T. Furuichi, and K. Mikoshiba. 2002. A novel recombinant hyperaffinity inositol 1,4,5-trisphosphate (IP_3) absorbent traps IP_3, resulting in specific inhibition of IP_3-mediated calcium signaling. *J. Biol. Chem.* 277:8106–8113.

Uhlen, P. 2004. Spectral analysis of calcium oscillations. *Sci. STKE.* 2004:pl15.

van der Wal, J., R. Habets, P. Varnai, T. Balla, and K. Jalink. 2001. Monitoring agonist-induced phospholipase C activation in live cells by fluorescence resonance energy transfer. *J. Biol. Chem.* 276:15337–15344.

Wakui, M., B.V. Potter, and O.H. Petersen. 1989. Pulsatile intracellular calcium release does not depend on fluctuations in inositol trisphosphate concentration. *Nature.* 339:317–320.

Wakui, M., Y.V. Osipchuk, and O.H. Petersen. 1990. Receptor-activated cytoplasmic Ca^{2+} spiking mediated by inositol trisphosphate is due to Ca^{2+}-induced Ca^{2+} release. *Cell.* 63:1025–1032.

Wang, S.S., A.A. Alousi, and S.H. Thompson. 1995. The lifetime of inositol 1,4,5-trisphosphate in single cells. *J. Gen. Physiol.* 105:149–171.

Woods, N.M., K.S. Cuthbertson, and P.H. Cobbold. 1986. Repetitive transient rises in cytoplasmic free calcium in hormone-stimulated hepatocytes. *Nature.* 319:600–602.

Xu, C., J. Watras, and L.M. Loew. 2003. Kinetic analysis of receptor-activated phosphoinositide turnover. *J. Cell Biol.* 161:779–791.

Yao, Y., J. Choi, and I. Parker. 1995. Quantal puffs of intracellular Ca^{2+} evoked by inositol trisphosphate in *Xenopus* oocytes. *J. Physiol.* 482:533–553.

Yoshikawa, F., M. Morita, T. Monkawa, T. Michikawa, T. Furuichi, and K. Mikoshiba. 1996. Mutational analysis of the ligand binding site of the inositol 1,4,5-trisphosphate receptor. *J. Biol. Chem.* 271:18277–18284.